Time-lapse seismic and AVO modelling, White Rose Field, Newfoundland

Ying Zou and Laurence R. Bentley

ABSTRACT

We have applied FluidSeis, well logs and AVO modelling to investigate the change in seismic response due to fluid substitution in the White Rose Field. The White Rose Field has a gas cap, an oil leg and a water drive. Three scenarios are presented. A water drive has water replacing the oil in the oil leg up to residual oil saturation. A gas drive has gas replacing the oil in the oil leg up to residual oil saturation. A final scenario has gas invading the upper half of the oil leg and water invading the lower half of the oil leg. Using PVT data and inferred post-production saturation, new sonic logs and density logs are generated. Synthetic seismic and AVO models are compared before and after production. Reflection coefficients at the gas-oil contact (GOC) and the oil-water contact (OWC) change in magnitude approximately 15%. The synthetics indicate that P-P and P-S AVO responses can be used to observe the changes in fluid distributions. The change in density due to fluid substitution appears to be the major factor in changing the seismic response. This study indicates that the White Rose Field is a good candidate for time-lapse seismic monitoring of fluid movements.

INTRODUCTION

Time-lapse seismic surveys have been used to monitor reservoir changes due to production. Time-lapse seismic monitoring of reservoirs is based on changing seismic response due to fluid substitution and pressure changes. The observable changes in seismic response can help locate bypassed oil and water- or gas-flood fronts (Sonneland et al., 1997, Li et al., 2001).

In this study, we predict the changes to seismic response due to fluid substitution in the White Rose Field, Newfoundland. White Rose is a large offshore field that has not been produced. Consequently, time-lapse seismic surveying may play an important role in the production of the field as it has in many North Sea fields. The change in seismic response due to fluid substitution is investigated in order to evaluate the usefulness of time-lapse seismic surveys at White Rose. We used FluidSeis (Zou and Bentley, 2001) to calculate changes in velocity and density due to fluid substitution. FluidSeis is based on the Gassmann equation and a modification of the procedure described by Bentley et al. (1999). The new velocity and density profiles are used to generate post-production synthetic seismograms that can be compared to pre-production synthetic seismograms. Zero-offset, P-P and P-S AVO responses have been compared.

WHITE ROSE STUDY

The White Rose field is located in Jeanne d'Arc Basin, offshore Newfoundland. Husky Oil drilled the White Rose L-08 well during the spring of 1999. The geology consists of a thick section of Tertiary shales separated from Cretaceous shales by an unconformity. Gas and oil were discovered in the underlying Cretaceous Avalon sands (Hedlin, 2000). Figure 1 shows the logs from L-08 exploration well.

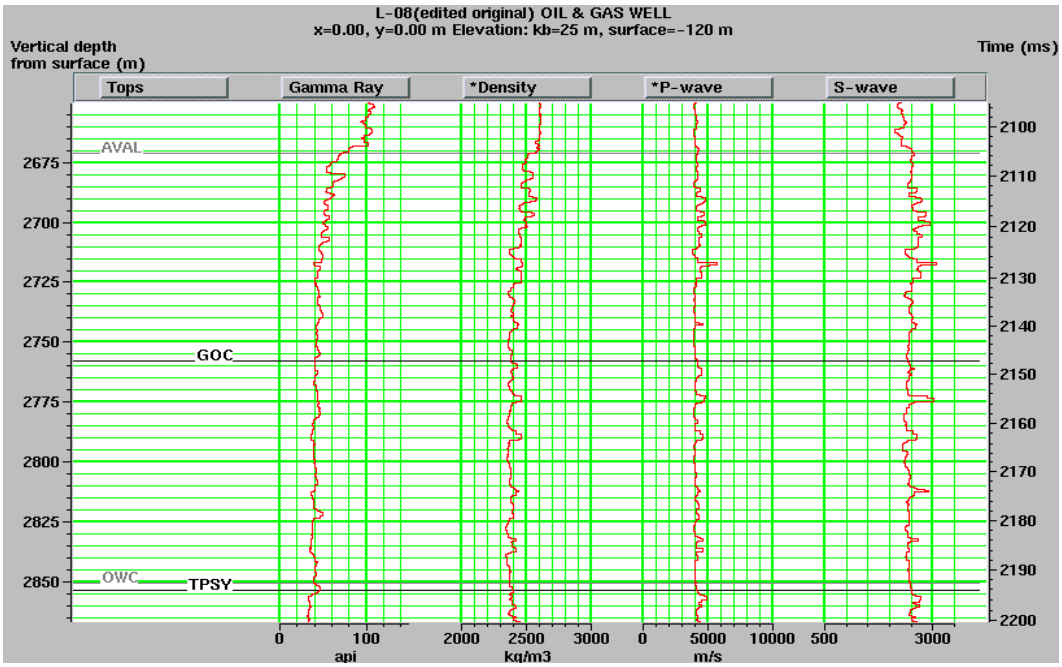

FIG. 1. The original logs from well L-08

The gamma ray log and density logs clearly separate Avalon sand from the overlying shale (Figure 1). A corridor stack from a down-hole VSP survey is shown in Figure 2. The parameters of the reservoir rock and PVT data are shown in Table 1. The White Rose Field has not been produced to date. In the following, we investigate the following three drive production scenarios.

(1) Gas drive through the entire oil leg. Oil is replaced by gas. Residual oil is 0.3 and connate water is 0.22.

(2) Water drive through the entire oil leg. Oil is replaced by water. Residual oil is 0.3 and there is no gas saturation.

(3) Half of the oil leg is replaced by gas and the other half is replaced by water.

All scenarios assume that reservoir pressure and temperature are maintained at the initial levels.

Table1. Reservoir parameters

Average porosity	0.19
Average connate water	0.20
Average oil saturation	0.80
Reservoir pressure	29.4 MPa
Reservoir temperature	106^{o}C
Gas oil ratio at P & T	122 SCF/STB
Oil API degree	31
Oil formation volume factor	1.37 BBL/STB
Specific gravity of gas	0.734

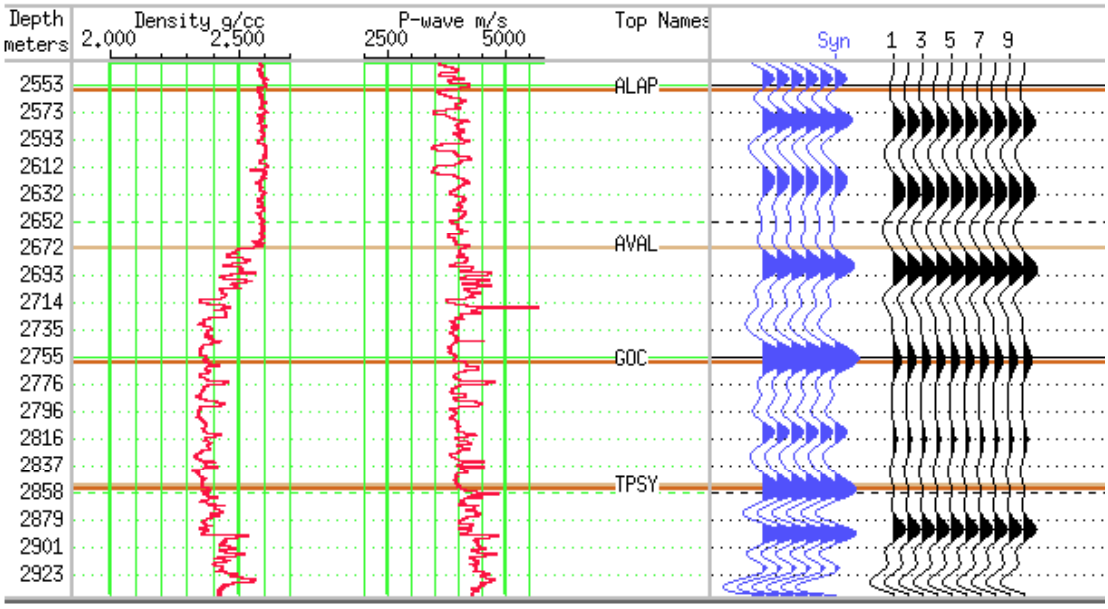

FIG. 2. The original logs, the synthetic trace (blue) and the VSP corridor stack (black).

RESULT ANALYSIS

FluidSeis was used to calculate new sonic and density logs to approximate the post-production reservoir conditions. The program can be found as part of the CREWES 2001 Research Report Software Release (Zou and Bentley, 2001). A wavelet was extracted from the VSP corridor stack, applied to the original logs and zero-offset synthetic traces were generated (Figure 2). Hampson-Russell's STRATA and AVO package are used to tie synthetic traces with corridor stack and to do AVO modelling.

The corridor stack and the original log synthetic traces match reasonably well. The main exceptions are the two cycles below the GOC, which are strong on the synthetic and weak on the corridor stack. Three new density logs and velocity logs for the three drive mechanisms were constructed using FluidSeis. Applying the wavelet from the corridor stack to the calculated logs, we obtained zero-offset synthetic seismic traces for the original logs, the gas-drive logs and the water-drive logs (Figure 3). The differences between the synthetics due to different drive mechanism are not very big but they are visible. The amplitude at the GOC decreased slightly in gas drive scenario and increased in water drive scenario. At the OWC the amplitude increased slightly in gas drive scenario and decreased. Table 2, 3, and 4 provide a summary of the changes due to fluid substitution. For gas drive, the bulk modulus decreases 2.3 %, but the P-wave velocity increases due to a 1.9 % decrease in density. The S-wave velocity increases 0.9 %. The velocity changes are small changes due to the large value of *Kd* compared to the pore fluid contribution to *Ku*. For the water drive case, the P-wave velocity increases 0.6 %, the S-wave average velocity decreases 0.5 % and the average bulk modulus increases 4.4 percent. Although the percentage change in density and velocity are small, they lead to changes in the reflection coefficients from the original GOC and WOC on the order of 15%. The zero-offset synthetic traces show visible amplitude changes due to fluid substitution which are consistent with the calculated change in reflection coefficient.

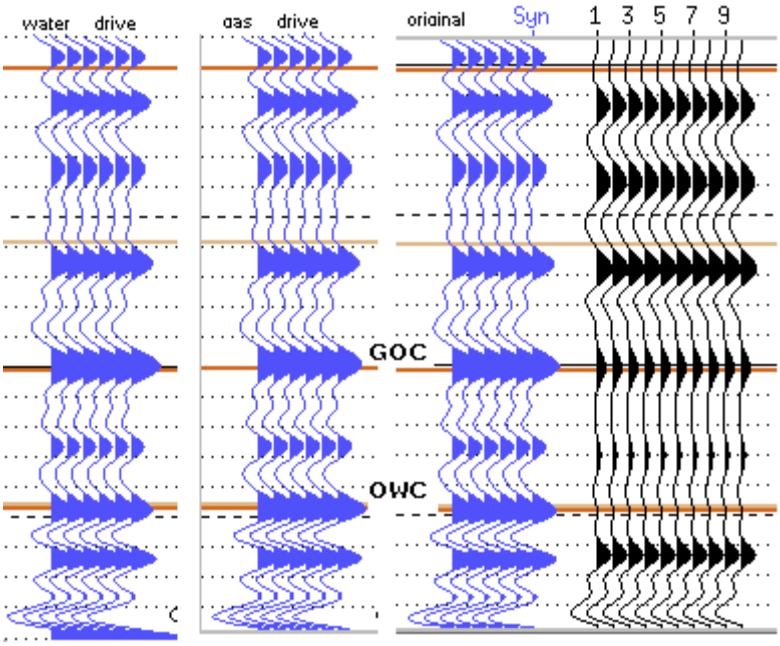

FIG. 3. Comparison of synthetics. From left to right, water-drive scenario, gas-drive scenario, original logs, and the corridor stack.

Gas drive	Ku(GPα)	ρ_u(Kg/m^3)	Vp(m/s)	Vs(m/s)	AIP(Kg/m^{2}s)
M	-.44	-43.85	15.74	23.64	-148851
std	.14		10.13	1.13	14463.7
%	-2.3	-1.9	.4	.9	-1.5
std	.009		.002	.0001	.002

Table 2. Mean (M) change, mean percentage change (%), and their standard deviation (std) in oil leg zone due to fluid substitution, gas drive case.

Water drive	Kμ(GPα)	ρ_u(Kg/m^3)	Vp(m/S)	Vs(m/s))	AIP(Kg/m^{2}s)
M	0.84	23.56	24.13	-12.43	157414
std	0.26		16.13	0.59	33322.5
%	4.4	1.0	.6	-.5	1.6
std	.017		.004	.0001	.004

Table 3. Mean changes (M), mean percentage change (%) and their standard deviation (std) in oil leg zone due to fluid substitution, water-drive case.

R_{coeff}	Original	Gas drive	Change (%)	Water drive	Change (%)
GOC	0.038	0.0311	-18.16	0.0447	17.63
OWC	0.0466	0.0550	15.27	0.0379	-18.67

Table 4. Reflection coefficients on GOC and OWC for gas drive and water drive case.

AVO effects were also studied. The modelling uses Zoeppritz equations in Hampson-Russell's AVO package. AVO effects are visible at the GOC and the OWC on the original well model synthetics (Figure 4). Positive reflection coefficients appear at both the GOC and the OWC. At the GOC the reflection coefficients increase with offset and at the OWC the reflection coefficients decrease with offset. Ostrander (1984) gave a detailed analysis on AVO as a function of the ratio of Poisson's ratio and the ratio of Vp (VR) across an interface. Although there is always a transition zone, we consider the ratio of the average values across the interface. The Poisson's ratio does not change much at the OWC, and Vp increases slightly across the OWC. Our cases correspond to VR=1.11 and DR=1.11 (Figure 5). At the GOC Poisson's ratio changes from small to large and Vp

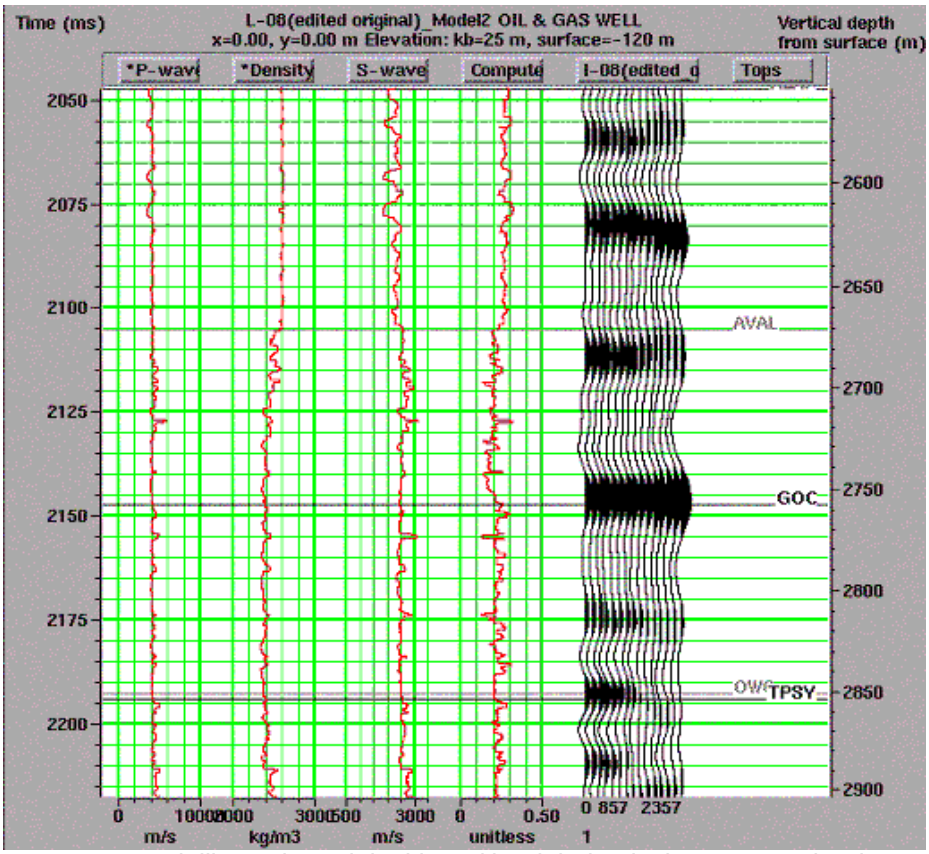

FIG. 4. AVO modelling using original logs (the right log is the computed Poisson's ratio).

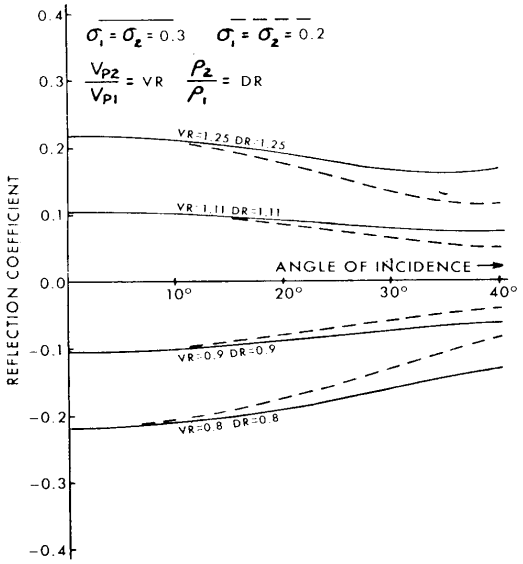

FIG. 1. Plot of *P*-wave reflection coefficient versus angle of incidence for constant Poisson's ratios of 0.2 and 0.3.

FIG. 5. P-wave reflection coefficients for constant Poisson's ratio across interface (after Ostrander 1984).

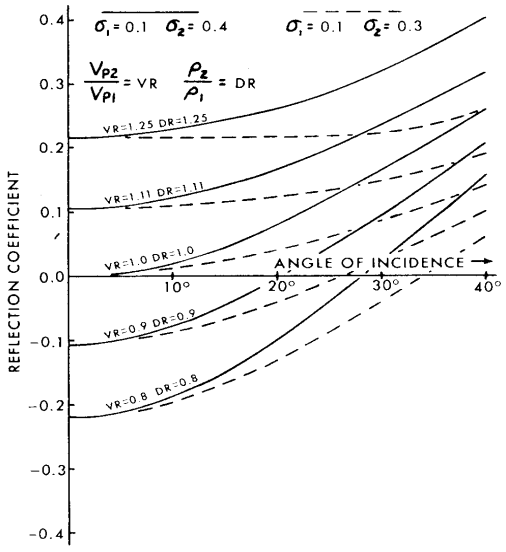

FIG. 3. Plot of *P*-wave reflection coefficient versus angle of incidence for an increase in Poisson's ratios across an interface.

FIG. 6. P-wave reflection coefficients for increasing Poisson's ratio across interface (after Ostrander 1984).

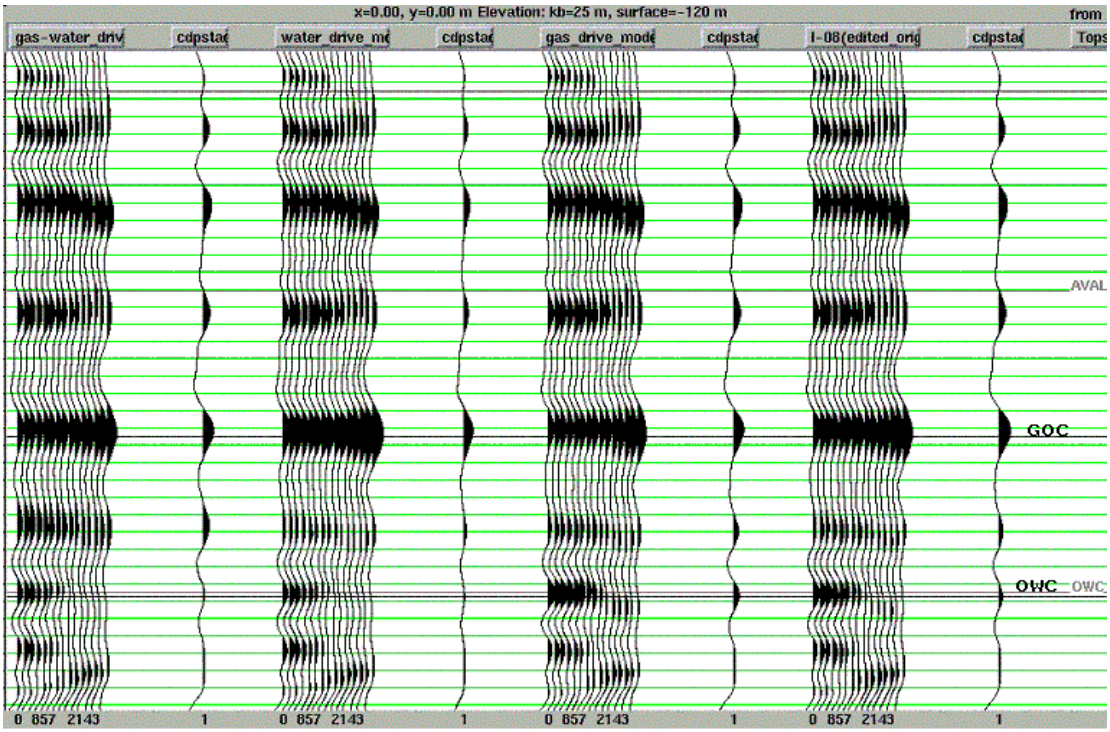

FIG. 7. AVO modelling for gas/water drive, water drive, gas drive and original log cases. The CDP stacked traces are plotted on the right of each AVO modelling traces.

increases. According to Figure 6 (Ostrander, 1984) the reflection coefficients should be increasing with offset. The GOC and OWC reflections seen in Figure 4 are consistent with these predictions.

Figure 7 compares the AVO effects of the three drive mechanisms with original log case. The fluid substitutions do not change the AVO trend but they do change the AVO amplitudes. In the gas drive scenario, the reflection at the GOC is weaker and the reflection at the OWC is stronger than the original case. After the water drive, the amplitude of the reflection at OWC is much smaller the reflection at the GOC is much stronger than original case. The GOC has become a water-oil/gas contact and the veclocity and density contrasts across the interface are greater. In gas/water drive scenario, a strong reflection develops in the center of the oil zone where the gas and water meet. The CDP stacked traces on Figure 7 show differences for the different fluid substitution cases. Time-lapse changes are more easily discerned on the AVO displays than the zero offset response.

The Matlab program SYNTH (Lawton and Howell, 1992, Margrave and Foltinek, 1995) was used to model AVO P-S converted wave responses. SYNTH is based on Zoeppritz equation. Figure 8, 9 and 10 shows the modelling results for original logs, logs from the gas drive case and logs from the water drive case, respectively. The wavelet used in the modelling is zero phase band limited (0-80 HZ) with a length of 200 ms. The reflection coefficient for the P-S converted wave (Bortfeld, 1961) is:

$$Rps = -\tan\theta_4\{(\frac{V_{p1}+V_{p2}}{V_{s1}+V_{s2}})(\frac{\rho_2-\rho_1}{\rho_2+\rho_1})+4[(\frac{V_{s2}-V_{s1}}{V_{s2}+V_{s1}})+\frac{1}{2}(\frac{\rho_2-\rho_1}{\rho_2+\rho_1})]\cos(\theta_1+\theta_4)\}$$

Using this equation, Hilterman (2001) presents a model with small velocity contrasts that are similar to our case. The P-S modelling results (Figure 8 - 10) have the same trend as his calculation (Figure 11, the second chart in the upper row). The reflection coefficient for the P-S wave increases from 0^o to about 20^o offset angle and then decreases with increasing offset. We see a similar trend in the P-S reflections of strengthening reflection with offset until a maximum strength is reached followed by decreasing reflection strength. Fluid substitution has not changed the character of the P-S AVO response at neither the GOC nor the OWC. However, amplitude changes are visible. Figure 12 shows the original and gas P-S wave synthetics and the original minus the gas substitution cases. Figure 13 shows the original and the water drive P-S synthetics and the original minus the water substitution cases. As expected, no difference exist above the GOC fort either case. In the gas case, the P-S wave shows a large decrease in the amplitude in the oil zone after gas substitution, but little change below the OWC. For the water drive case, a significant reduction in P-S amplitude exists within the oil zone, but it is less than in the gas case.

CONCLUSIONS

The substitution of reservoir oil by gas and water can cause changes in seismic response that can be interpreted in terms of changes in fluid distributions due to production. Synthetic modelling results predict that gas or water drives will cause changes to the zero-offset reflection coefficients on the order of 15%. Changes to the P-P AVO displays are more dramatic than changes to the stacked traces. Modeled P-S converted wave AVO effects are also significant.

A major source of uncertainty exists in the modelling of the bulk modulus of the fluid mixtures. The appropriate average for fluid bulk modulus ranges from a minimum (harmonic average) for homogeneous fluid saturation to a maximum (arithmetic average) for patchy saturation. Arbitrarily, we have used the average of these two values. Due to the relatively high value of the dry bulk modulus, *Kd*, the influence of the fluid saturation is relatively small. The undrained bulk modulus changed –2.3 % and +4.4% for the gas drive and water drive, respectively. Since it is the square root of the bulk modulus that influences the velocity, these minor changes have little influence on the velocity. Velocity variations are quite small, less than 1%. Consequently, uncertainty in the fluid mixture bulk modulus is not a major problem. It appears that most of the change in seismic response is due to the change in acoustic impedance caused by fluid replacement induced changes to the density.

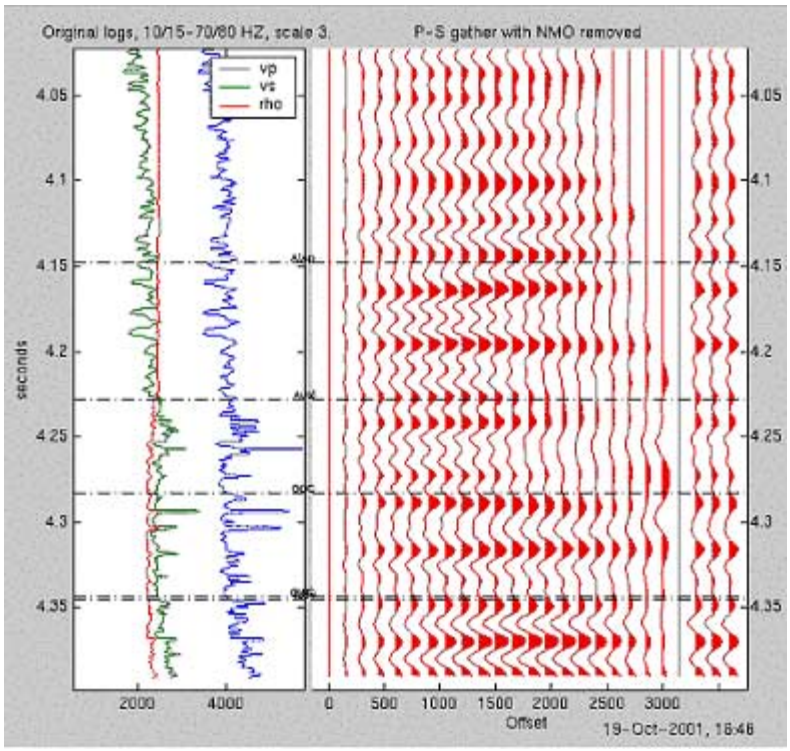

FIG. 8. Original logs and P-S wave AVO modelling.

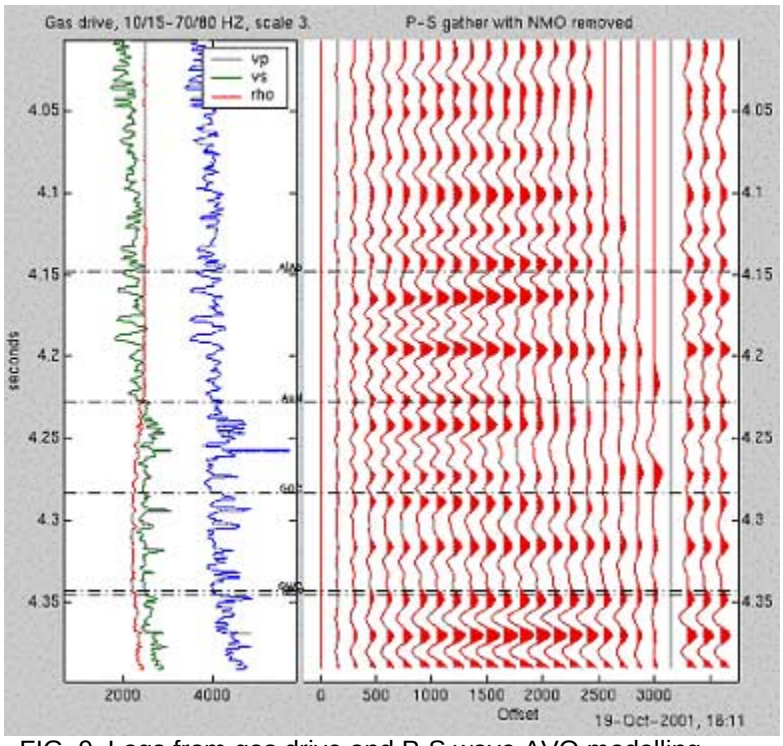

FIG. 9. Logs from gas drive and P-S wave AVO modelling.

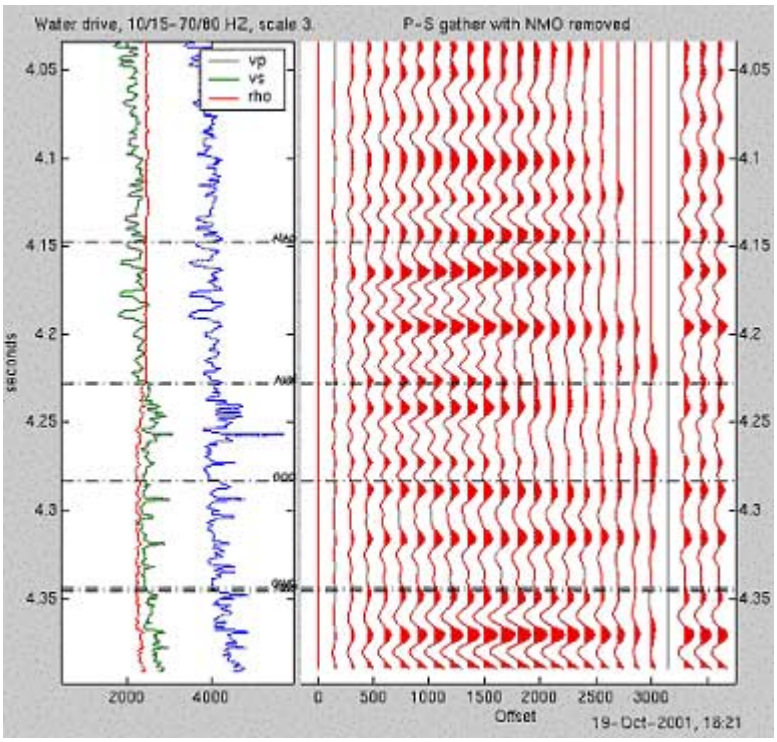

FIG. 10. Logs from water drive and P-S wave AVO modelling.

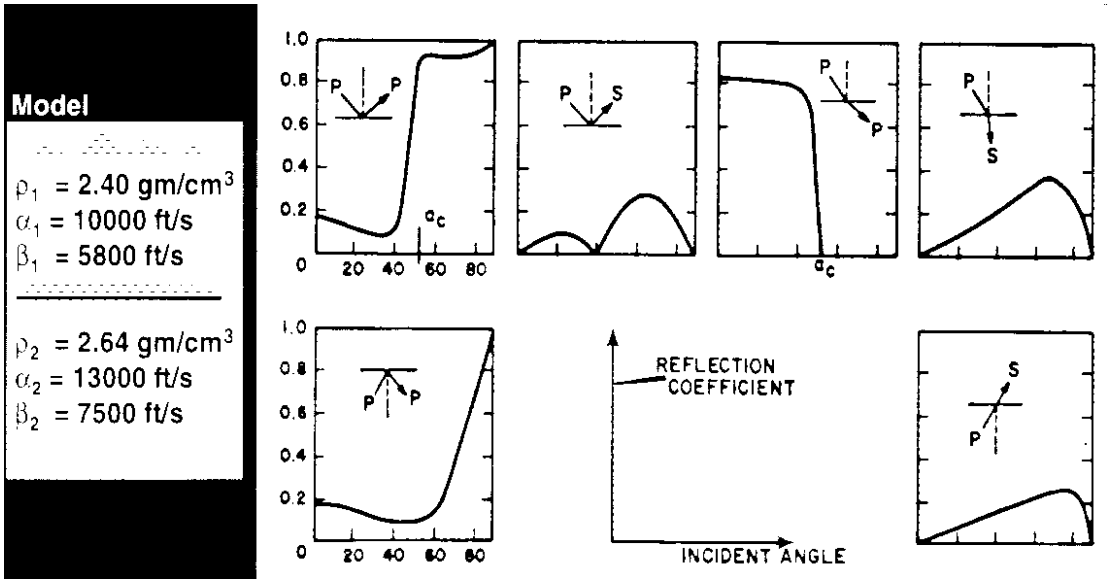

FIG. 11. Amplitude vs. Incident Angle, Small Velocity Contrast (after Hilterman 2001)

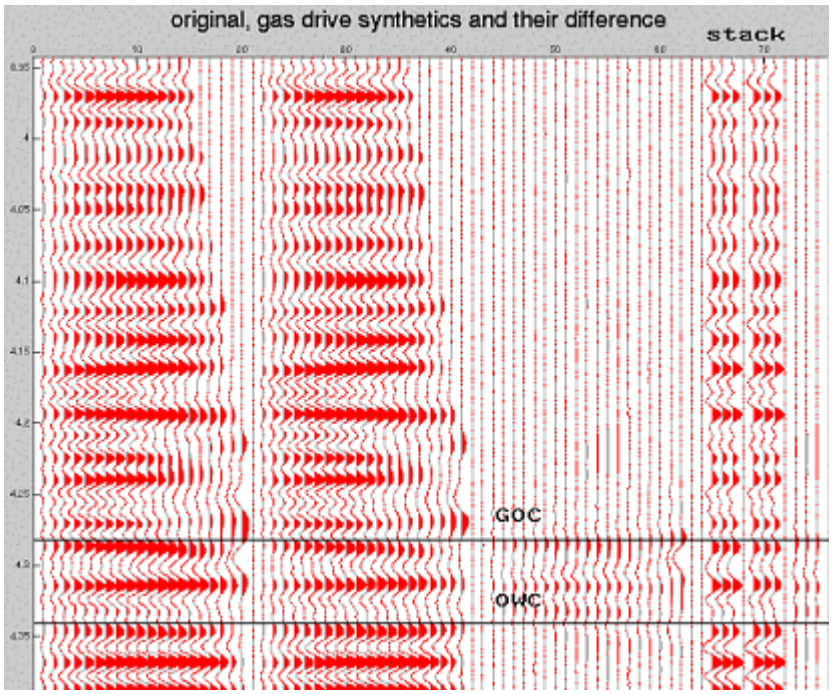

FIG. 12. P-S wave synthetic traces for original logs, gas drive logs and their difference.

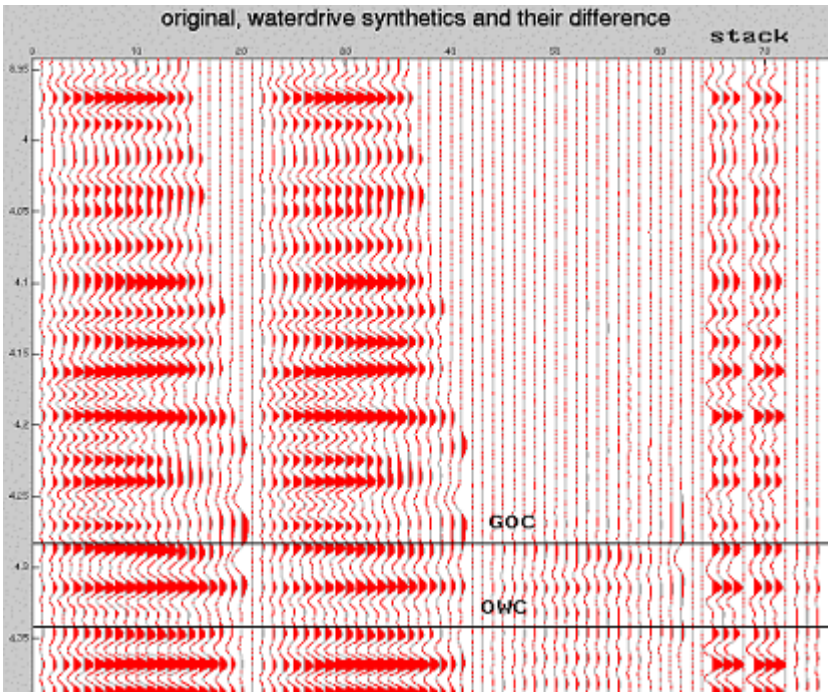

FIG. 13. P-S wave synthetic traces for original logs, water drive logs and their difference.

This study indicates that the White Rose Field is a good candidate for time-lapse seismic monitoring of fluid movements. The change in density due to fluid substitution appears to be the dominant cause of seismic response change. P-P and P-S AVO responses appear to be particularly useful monitoring tools. Further work should include adding noise to the synthetic traces, AVO attribute analysis, accounting for possible changes in pressure within the reservoir and exploring additional by-passed oil and pressure maintenance scenarios.

ACKNOWLEDGEMENTS

We thank the CREWES sponsors and NSERC for their support of this research. A special thanks goes to Larry Mayo and Larry Mewhort at Husky Oil for providing the data used in this study. We also thank Hampson-Russell for their software.

REFERENCES

Bentley, L.R., Zhang, J., and Lu, H., 1999, Four-D Seismic Monitoring Feasibility: CREWES Research Report, 11, 761-776.

Bortfeld, R., 1961, Approximation to the Reflection and Transmission Coefficients of Plane Longitudinal and Transverse Waves: Geophys. Prosp., 9, 485-503.

Hedlin, K., 2000, Pore Space Modulus and Extraction Using AVO: SEG GeoCanada 2000 Convention Abstract.

Hilterman, F.J., 2001, Seismic Amplitude Interpretation: 2001 Distinguished Instructor Short Course Note.

Lawton, D.C. and Howell, T.C., 1992, P-P and P-SV synthetic stacks: Expanded Abstracts, 62nd Annual SEG Mtg., 1344-1347.

Li, G., Purdue, G., Weber, S., and Couzens, R., 2001, Effective Processing of Nonrepeatable 4-D Seismic Data to Monitor Heavy Oil SAGD Steam Flood at East Senlac, Saskatchewan, .Canada: The Leading Edge, 20, No. 1, 54-62.

Margrave, G.F. and Foltinek, D.S., 1995, Synthetic P-P and P-SV cross-sections: Annual CREWES Research Report, 7.

Ostrander, W.J., 1984, Plane-wave Reflection Coefficients for Gas Sands at Nonnormal Angles of Incidence: Geophysics, 49, 1637-1648.

Sonneland, L., Hafslund Veire, H., Raymond, B., Signer, C., Pederson, L., Ryan, S., and Sayors, C., 1997, Seismic Reservoir Monitoring on Gullfakes: The Leading Edge, 16, No. 9, 1247-1252.

Zou, Y. and Bentley, L.R., 2001, “FluidSeis” user’s guide (a Matlab fluid substitution program): CREWES Research Report, 13.